Heterodyne Detection using Frequency-Modulated Continuous-Wave LiDAR.

Fredrik Johansson

Thesis submitted for the degree of Master of Science
Project duration: 4 months, VT20 (FYSM30)

Supervised by: Robert Lanner & Olle Lundh

Abstract

Light Detection and Ranging (LiDAR) is a technique that can change the way automated systems interact with their environments. The most common LiDAR systems used in industry today are based on the concept of Time-of-Flight (ToF) and utilizes pulsed lasers. Coherent LiDAR, such as Frequency-Modulated Continuous-Wave (FMCW) LiDAR, which operates with a chirped continuous-wave laser, offers advantageous resolution and precision compared to ToF LiDAR. The main drawbacks for FMCW LiDAR are the complexity and cost of the system. The goal of this project was to improve the understanding of the fundamentals and the operational functions of FMCW LiDAR systems. This was done by designing and constructing a FMCW LiDAR that can perform measurements up to a distance of $10\,\mathrm{m}$. Furthermore, by analyzing the individual components included in a FMCW LiDAR system, possible options to improve the measurement precision was investigated. Finally, distance measurements were made to evaluate the performance of the final construct.

Contents

1 Introduction

In modern society, the surroundings are in rapid transformation. Cars, robots and smartphones have become tools for modern humans and everything is becoming more integrated, more useful and smarter. This does not only put high demands on individuals to adapt to new devices and techniques, but also requires that systems and computers understand, interpret, and predict the actions and needs of the users as well as their environments.

An important part to cope with these requirements is the ability to recognize objects and movements in the surrounding environment in real-time. To be able to perform this recognition, data has to be obtained. One type of device that can perform this task of obtaining data is sensors and the field of sensors has completely exploded with new companies and products using various techniques. One specific technique that has gotten much attention in recent times is LiDAR. LiDAR is an acronym for "Light Detection and Ranging" and is a technique that measures distance and velocity of a target by illuminating it with a laser and measuring the reflected light with a sensor. The technique is often referred to as "laser radar" since it utilizes many of the same features as radar does [1, 2].

The applications in which LiDAR can be used are plenty and extremely varying. Topography mapping, biomass measurements, spectroscopy, and three-dimensional imaging are only some of these applications and in the autonomous vehicles industry, distance and velocity measurements, in particular, are areas of importance [1]. In this industry LiDAR could aid the vehicles to detect obstacles and allow them to navigate the streets safely and companies are therefore spending millions of dollars to integrate optoelectronics and LiDAR's into their systems [3].

This study will go deeper into a specific type of LiDAR, namely Frequency-Modulated Continuous-Wave (FMCW) LiDAR. The FMCW LiDAR most commonly utilizes a linearly FMCW laser instead of pulsed laser radiation, which otherwise is common for LiDAR applications. The FMCW LiDAR has also started a shift in the wavelengths that are used for detection. Currently, a wavelength around 905 nm has been the most commonly used, but through technical development in the telecom industry a drive towards 1550 nm has emerged [1]. The wavelength of 1550 nm has the advantages that there are both excellent detectors and fiber-light sources with high performance available and is also eye-safe as it is not focused on the retina.

This project is, as previously mentioned, focused on LiDAR. In section 2 the fundamentals and operational functions of FMCW LiDAR systems will be investigated through literature studies. The project will then continue with an attempt to design a LiDAR structure to get first hand knowledge of the difficulties that are involved in the design of an optical system, which is presented in section 3. In section 4, the produced system is finally used to measure range through homodyne detection, which is a special case of heterodyne detection. The main goal of the project is to increase the understanding of FMCW LiDAR systems and give a hint if such systems could be used in electronic products. The project is in collaboration with SAAB Dynamics, a company operating in the defense industry. Therefore, possible applications in their products should be taken into account.

2 LiDAR

The use of light for range finding has been around for as long as the laser itself. The first LiDAR was developed in 1961, the year after the first laser was demonstrated, and has since then emerged as a measurement tool in various technological fields. LiDAR is generally separated into two different types: *Time-of-flight* and *Coherent* LiDAR [1].

The fundamental principle of Time-of-flight (ToF) LiDAR consists of a pulse being sent out in a direction, hitting a target, and being reflected towards the source. It is then possible to determine the distance to the target using the time delay of the reflected light for traveling a longer distance than another pulse of light used as reference according to [4]:

$$R = \frac{c \cdot \tau_d}{2},$$ (1)

where R is the range, c is the speed of light and τ_d is the round-trip delay.

Coherent LiDAR also sends out light and detects the light that is reflected, but instead of pulses it utilizes a frequency-modulated continuous-wave (FMCW) laser. Due to the use of the FMCW laser it is often referred to as FMCW LiDAR, which will be used in this report. The received back-reflected light is mixed and superimposed with a local oscillator [1]. This process allows for not only determining the distance to the object of which the light is reflected but also its velocity relative to the LiDAR through Doppler-shifts [4].

2.1 FMCW LiDAR

As mentioned in the previous section, FMCW LiDAR is based on modulation of the frequency of the laser that is used for detection. This modulation is referred to as chirp and is an important characteristic of FMCW LiDAR. Most commonly, the chirp is linear and increases from a base frequency, f_0, to a maximum frequency, f_{max}, over some period of time, T. This process of increasing frequency is called "up-chirp" and is often followed by a "down-chirp", which is a decrease from f_{max} to f_0 over the same period T [5, 6].

The operative process of the FMCW LiDAR implements the principles of interferometry to determine an unknown length. The unknown length that is to be determined acts as one arm in an asymmetric interferometer such as a Mach-Zehnder interferometer (MZI). The light from the chirped laser is split up into two paths, one which is used as signal and one which is called the local oscillator (LO). The signal beam is directed towards a target where the transmitted beam is reflected by the target. This reflected light is then collected as the signal, mixed with the LO such that they interfere and is then detected by a photodetector (PD) [7, 8, 9]. When interfering on the detector the beams have traveled different optical path length. This gives rise to a time-delay between them. This time-delay results in the LO and the signal having different frequencies and as they interfere a beat frequency, equal to their difference in frequency, is generated. The beat frequency allows for determining the distance to the target as the difference in optical path arises due to the distance to the target [8].

2.1.1 Range and Velocity measurements

The structure of a FMCW LiDAR often resembles a MZI as illustrated in figure 1. Such LiDAR results in an intensity response upon the PD with a sinusoidal behavior with a free-spectral-range (FSR) that can be calculated according to equation 2. For a MZI, the FSR is defined as the distance between adjacent constructively interfering optical frequencies:

$$\Delta\nu_{FSR} = \frac{c_0}{|L_{LO}n_g - 2Rn_0|},\tag{2}$$

where c_0 is the speed of light in vacuum, L_{LO} the length of the LO, n_0 the refractive index of air and n_g is the group index of the fiber of the LO [8, 10].

The $\Delta\nu_{FSR}$ can be used when measuring range by sweeping the laser over numerous FSR of the interferometer. Utilizing a fixed linear sweep allows for the detection of interference fringes. The fractional number of these fringes indicate the delay difference between the different optical paths along the arms in the interferometer and thus the distance to the target [8].
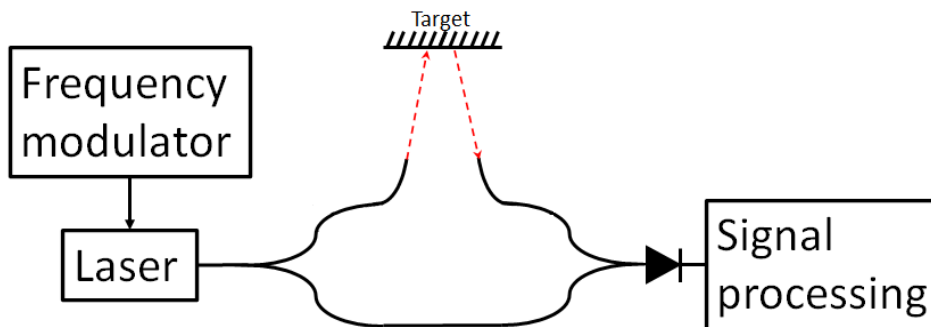

Figure 1: Schematic of LiDAR structure utilizing the features of MZI. The LiDAR consists of a frequency modulating instrument, laser, light guiding, photodetector and signal processor. The light guiding in this schematic is illustrated as fiber optical cables.

Assuming a static target, the signal reaches the receiver after the round-trip delay $\tau_d = \frac{1}{FSR}$, similar to the ToF LiDAR. As mentioned, the delay between the signal and the LO results in a beat frequency, f_{beat}. For a linearly modulated frequency, this difference is constant and directly proportional to the time delay [4]. This proportional relation follows $f_{beat} = \gamma \cdot \tau_d$, where $\gamma = (\Delta f_{laser})/T$ is the chirp-rate i.e. the frequency modulation per unit time, where $\Delta f_{laser} = f_{max} - f_0$. Inserting this expression into equation 1 allows for determining the distance to the target according to equation 3 [8, 9]:

$$R = \frac{c \cdot \tau_d}{2} = \frac{c}{2}\frac{f_{beat}}{\gamma},\tag{3}$$

where f_{beat} can be either positive or negative depending on if the frequency is "up-chirped" or "down-chirped", illustrated in figure 2.
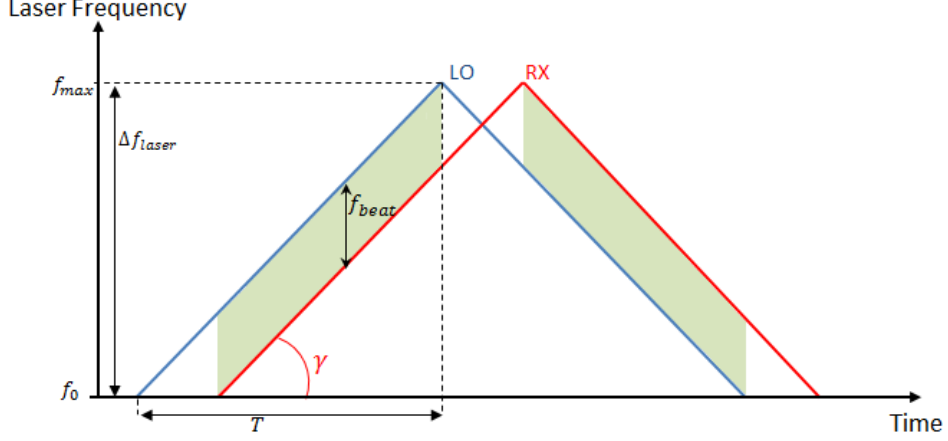
Figure 2: The figure illustrates the beat frequency that results from frequencies for the local oscillator (LO) and the back reflected signal (RX) when interfering onto the photodiode. As can be seen the signal is delayed with a certain time, which generates a difference in the frequency between the LO and signal. This difference is called the beat frequency.

By performing a fast Fourier transform (FFT) on the output from the PD, a spectrum with x-axis directly corresponding to the difference in the optical path between the two arms in the interferometer, can be acquired. This becomes very computationally efficient and therefore allows for faster response time for the system [9, 10]. However, the precision of the measurement can vary a lot and is extremely dependent on the characteristics of the laser. The precision is often referred to as the "Fourier resolution", equation 4, and is the resolution of the time delay [8]:

$$\delta\tau = \frac{1}{\Delta f_{laser}}, \tag{4}$$

This definition of precision originates from the ability to separate targets from each other. Targets that give rise to delay differences which are smaller than $\delta\tau$ can not be separated from each other. Thus, by increasing the swept frequency range of the laser, the resolution of the FMCW LiDAR can be greatly increased. This is one of the main advantages compared to ToF LiDAR as the resolution is principally not limited by measurement electronics [2, 8, 9].

When introducing a velocity, v, to the target along the line of sight of the LiDAR, the light will undergo a frequency shift due to the Doppler effect. This frequency shift is dependent on the magnitude of the velocity and the direction of movement relative to the LiDAR. The observed frequency of the light after the Doppler shift, f_d, is defined according to equation 5 [5, 10]:

$$f_d = \left(\frac{c}{c \pm v}\right) f_c, \tag{5}$$

where f_c is the original frequency of the laser and c is the speed of light. $+v$ corresponds to target moving away from and $-v$ moving towards the LiDAR. The Doppler shift can be determined by calculating $f_d - f_c$.
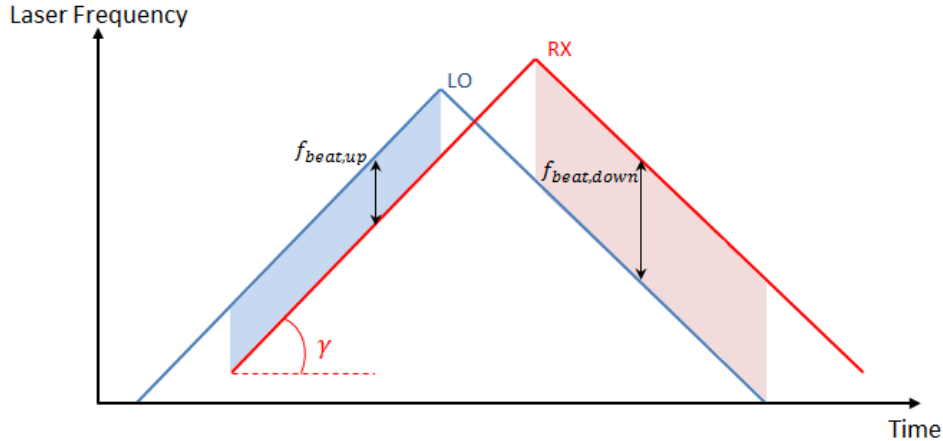
4

Figure 3: The figure illustrates the effect the Doppler shift has on the beat frequency that occur when the local oscillator (LO) and the reflected signal (RX) interfering onto the photodiode. As the target is moving in a certain direction, a down- or up-shift in the frequency occurs. This shift causes the beat frequency to be different depending on if the LiDAR is in a down- and up-chirp. By knowing the beat frequency for a static target it is thereby possible to calculate the velocity of the target as well as the direction it travels along the line of sight of the LiDAR.

This shift is seen in the observed beat frequency, where the signal is shifted with some amount depending on the velocity of the target. As a result of this, the beat frequencies measured during the up-chirp and down-chirp differ from each other, illustrated in figure 3 [8, 9].

2.2 Optical Heterodyne detection

Heterodyne detection was originally developed in the field of radio waves and microwaves where a weak input signal is mixed with a "local oscillator wave". The mixed product is then detected after filtering out the LO and the original signal. The detected frequency corresponds to the sum or difference of the frequencies of the signal and the LO. This method is in many ways similar to how optical heterodyne detection operates, where an optical signal is mixed with a LO to produce a mixed electrical signal. Instead of filtering the input, the detection is simply done on the linearly superimposed waves using a square-law photodetector, most often a PD [5, 11].

Fundamentally, the signal and LO can be seen as two separate monochromatic waves of frequency ν_S and ν_L, where S denotes the signal and L the local oscillator. The intensities of these waves are then I_S and I_L, respectively. This gives a complex wavefunction at some time in space according to equation 6, in which the $\bar{r}$ dependence has been suppressed [10]:

$$U(t) = \sqrt{I_S} exp\left(j2\pi\nu_S t + \varphi_s\right) + \sqrt{I_L} exp\left(j2\pi\nu_L t + \varphi_L\right) \tag{6}$$

Here φ_S and φ_L are the phases of the two monochromatic waves, respectively.

As these two waves interfere with each other, they can be seen as a single polychromatic wave and thus have an intensity of the absolute square of the complex wavefunction. Applying this to equation 6 gives the expression for the intensity according to equation 7 [9, 10]:

$$I(t) = |U(t)|^2 \simeq I_S + I_L + 2\sqrt{I_S I_L} \cos[2\pi(\nu_S - \nu_L)t + (\varphi_S - \varphi_L)], \tag{7}$$

where $\nu_I = \nu_S - \nu_L$ is called the intermediate, or beat, frequency.

PDs are responsive to the optical intensity and according to equation 7, this makes PDs sensitive only to the difference frequency, unlike radio and microwave detectors, which can also detect the sum. The optical power, P, incident on the PD is calculated through the integral of the intensity over the detector area and becomes equation 8 [9, 10].

$$P = P_S + P_L + 2\sqrt{P_S P_L} \cos[2\pi(\nu_S - \nu_L)t + (\varphi_S - \varphi_L)] \tag{8}$$

The third term in equation 8 above, varies with time and has a phase of $\varphi_S - \varphi_L$. The difference frequency, ν_I, can be several orders of magnitude smaller than the individual frequencies of the signal and LO if the beams are close in frequency [8, 10].

The generated photocurrent i, is proportional to the incident photon flux, Φ. Assuming small difference in frequency between signal and LO and thus ν_I much smaller than ν_S and ν_L, the superimposed light is quasi-monochromatic with a photon flux following equation 9 [9]:

$$\Phi = P/h\bar{\nu}, \tag{9}$$

where P is the optical power, h is Planck constant, and $\bar{\nu} = (\nu_S + \nu_L)/2$. As can be seen from equation 9, the photon flux is directly proportional to the optical power [10], this results in a mean photon current of equation 10:

$$
\begin{aligned}
\bar{\imath} = \eta e \Phi &= (\eta e P/h\bar{\nu}) \\
&= (\eta e P_S/h\bar{\nu}) + (\eta e P_L/h\bar{\nu}) + 2(\eta e/h\bar{\nu})\sqrt{P_S P_L} \cos\left[2\pi\nu_I t + (\varphi_S - \varphi_L)\right] \\
&= \bar{\imath}_S + \bar{\imath}_L + 2\sqrt{\bar{\imath}_S \bar{\imath}_L} \cos\left[2\pi\nu_I t + (\varphi_S - \varphi_L)\right],
\end{aligned} \tag{10}
$$

where e is the electron charge, η the quantum efficiency of the detector and $\bar{\imath}_S$ and $\bar{\imath}_L$ are the photocurrents generated by the signal and LO individually. Usually the LO is much stronger than the signal, which allows for neglecting the first term and thus get equation 11 [10]:

$$\bar{\imath} \approx \bar{\imath}_L + 2\sqrt{\bar{\imath}_S \bar{\imath}_L} \cos\left[2\pi\nu_I t + (\varphi_S - \varphi_L)\right] \tag{11}$$

In equation 11 the second term is carrying the useful information. If $\bar{\imath}_L$ and φ_L are known, which are the amplitude and phase of the LO, it is possible to determine the amplitude and phase of this second term. The information-containing variables $\bar{\imath}_S$ or φ_s, which are the amplitude and phase of he signal, are generally varying functions of time. Compared to the difference frequency ν_I, these variations are slow, as illustrated in figure 4 [9].
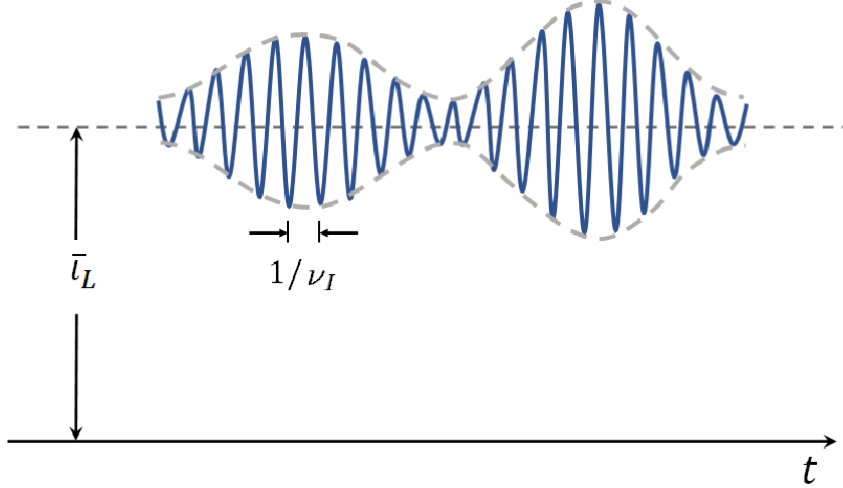
Figure 4: The figure illustrates the photocurrent generated by heterodyne detection. The information-containing variables $\bar{\imath}_S$ or φ_s can be seen as the envelope function with larger variation in time and compared with the difference frequency ν_I [10, p. 1114].

Homodyne detection, that is used in this project, is a special case of heterodyne detection where the signal and local-oscillator have the same frequency ($\nu_S = \nu_L$). By phase-locking the LO such that $\varphi_L = 0$, the photocurrent can be written as [10]:

$$\bar{\imath} = \bar{\imath}_L + 2\sqrt{\bar{\imath}_S \bar{\imath}_L} \cos \varphi_S, \tag{12}$$

where the amplitude or the phase modulation is achieved by varying the current $\bar{\imath}_S$ or the phase φ_S, respectively.

2.2.1 Light source

The lasers used in LiDAR systems are of a large variety both in the type of laser as well as the wavelength of the outgoing light. The optimal source should operate in single mode, have long coherence length and high output power. However, in the early designs of LiDAR systems the most used type of laser was a pulsed laser that emits light at 905 nm. This design has severe limitations regarding range as well as the high cost of the components in the system [1], the latter will be treated further in section 3.1. Another problem with this wavelength range is the interference from solar radiation and other surrounding light sources. These surrounding light sources interact with the detector in a way that reduces the sensitivity of the LiDAR significantly and restricts the usage in certain conditions. Furthermore, a wavelength of 905 nm invites a problem of eye-safety when the systems are introduced into society as this wavelength is focused on the retina [2].

As of lately, a shift towards laser with a wavelength of 1550 nm has become noticeable. One reason for this shift is that the wavelength range of 1550 nm allows for the use of a higher intensity while still being safe for the eyes of people in the surroundings, further developed in section 2.3.1. Additionally, as the telecom industry has gone through a rapid growth the last century, optical components for a wavelength of 1550 nm have decreased significantly in price and thus also made it a more interesting area for LiDAR development [6, 12].

One type of component from the telecom industry that is particularly interesting is diode lasers. Diode lasers, or laser diodes, are semiconductor devices in which a diode is directly pumped with an electrical current [12]. The pumping creates a lasing condition at the junction between the two different semiconductor materials (p-type and n-type) that the diode is designed for. The "p" side material contains an excess of holes, while the "n" side material contains an excess of electrons in the outer shells. This allows electrical current to pass through the junction of the p- and n-type material (p-n-junction) in only one direction [10]. Applying a voltage over the junction, allows for the recombination of these excess electrons and holes, and due to the drop of the electron from a higher energy level to a lower one, photons are emitted. This process is called spontaneous emission. As the photon from the spontaneous emission travel through the junction region there is a probability for it to interact with an excited electron in the material of the diode. The interaction causes the electron to drop to a lower energy level. The energy that is released due to this drop between energy levels is emitted as another photon with the same phase, frequency, polarization, and direction of travel of the incident photon. This is called stimulated emission and is one of the fundamental principles in lasers [10].
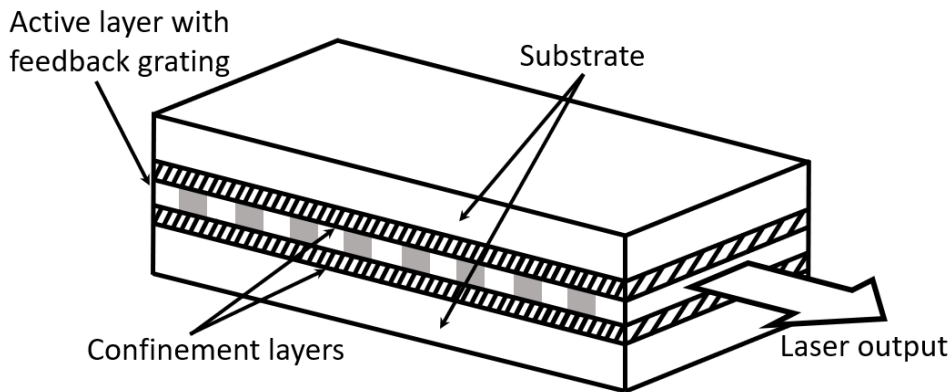

Figure 5: The figure is a schematic of the structure of a DFB laser diode. The structure consists of alternating p- and n-type semiconductor layers which only allows current flow in one direction. This results in a lateral confinement which cause the active layer to locate along the longitudinal direction. Following the active layer there is a built in periodical structure of various refractive indexes. This periodic structure acts as a grating reflecting back light which has a wavelength that corresponds to twice the length of the period of the grating. This causes only a single wavelength to be fed back to the gain region and lase.

There are numerous different laser diode structures, which create p-n-junction by layering p- and n-type material in different ways. The laser diode that was used in this project is a Distributed-feedback (DFB) laser diode [10]. DFB laser diode is a laser diode designed with hetero-structure of alternating p- and n-type material layers, illustrated in figure 5. These layers allow current flow only in the vicinity of the active region, where the photons are emitted, of the device. This restriction in current flow introduces lateral confinement. The active region is located along the longitudinal direction and has a periodically change in refractive index which acts as a diffraction grating. This grating structure results in back reflection of light which has a wavelength that corresponds to twice the length of

the period of the grating. If the end of this periodic structure is anti-reflection coated two longitudinal modes are supported by the structure and thus causes two wavelengths to lase. By applying a high reflectivity coating to the back end of the laser one of these can be suppressed. The coating leads to the DFB laser being quarter-wave shifted and reflected on itself. As a result of this only a single wavelength is fed back to the gain region. Thus, DFB laser diodes emit light of only a single wavelength and tend to be spectrally stable [9, 10].

The materials used in the laser diode affects the wavelength that is emitted. This comes from that the, previously mentioned, excited electrons are in different energy levels in different materials. As a result in these differences in energy levels, the photons emitted through the stimulated emission process will be of different energies. Thus, by constructing the laser diode with material with electrons in certain energy levels, it is possible to get emitted light of specific wavelengths [10].

2.2.2 Balanced photodetection

For optical systems working with lower input-signals, noise can be a large problem. To cope with these difficulties with noise, balanced photodetection was developed. The technique is primarily used for detecting differences between two optical input-signal and simultaneously suppressing fluctuations [13].

A simple balanced photodetector is composed of two PDs as well as a transimpedance amplifier (TIA). The PDs are connected in series such that the photocurrents produced by them cancel each other if equal. The cancellation method is called common-mode rejection ratio (CMRR) and is quantified in dB. Any difference in the photocurrents is sent to the TIA, which converts it to a voltage proportional to the difference. This voltage is then the output from the balanced photodetector [13].

During this project a balanced photodetector was used to measure intensity after a 50/50 beam splitter. Such balanced photodetector can obtain both the difference and the sum of the photocurrents from the PDs. Both the difference and the sum are then sent to an instrument that allows for analysis of the spectrum. The sum signal represents the intensity noise of the light source in a similar way as obtained by a regular PDs, while the difference signal indicates the shot noise level. This type of balanced photodetector allows for a comparing shot noise with laser noise and thus enables detection of signals below the shot noise. As a result, the noise performance can be improved significantly [7].

2.2.3 Frequency modulation

To vary the optical output from a DFB laser diode, the electric drive current, i.e. the amount of amperage sent through the diode, is often used. By directly modulating the drive current it is possible to modulate the intensity of the outgoing light and by doing so also the frequency. A typical laser diode's output optical power versus drive current can be seen in figure 6. As can be seen the output optical power varies as a function of the drive current. When biased below a threshold current, I_{th}, the output power is very low. But as the current increases over the threshold the output optical power increases significantly and shows an exponential behavior until the equilibrium value is reached and

the relation becomes linear [7, 10]. The threshold currents lie typically in the range of 25–250 mA and the output powers are typically in the range of 1–10 mW, depending on the laser diode.

Associated with the changes in the intensity as the drive current is varied, a change in frequency occurs. This has resulted in frequency modulation being realized by modulating the drive current. Changes in the drive current affect the lasing wavelength, and thus the frequency, in two different ways: thermal and plasmatic [5, 7].
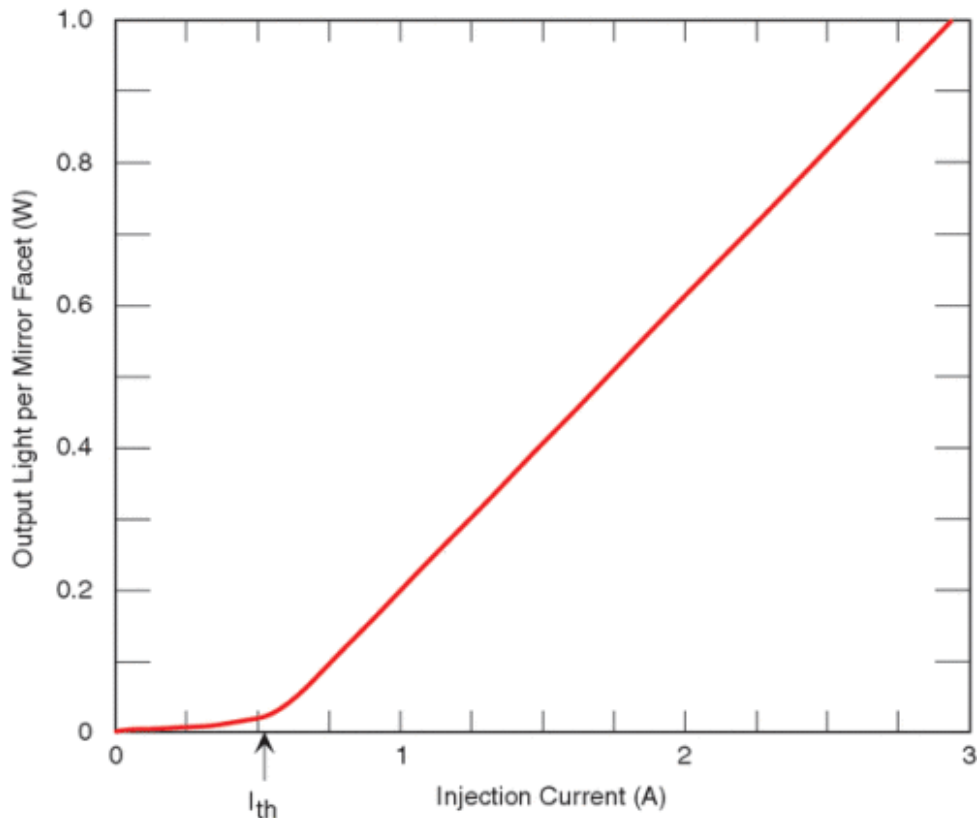

Figure 6: The figure illustrates the general behavior of a DFB laser diode. The optical power is typically low until the drive current reaches the threshold current, I_{th}. It then experiences an exponential increase until it reaches equilibrium and shows a constant relation. The threshold current is typically in the ranges of 25-250 mA [14]

The thermal effects have an impact on both the dimensions of the material and the gain in the material. As the temperature increases the relative length of the cavity changes. The relative change in cavity length results in a different periodicity in the grating in the active region in the diode. This causes the lasing condition to change as the lasing wavelength corresponds to twice the length of the period of the grating, as described in section 2.2.1.

With an increased drive current the gain will increase resulting in a larger population inversion, which is the number of electrons in excited states in the laser diode. Furthermore, as the population inversion increases the electrons in the excited states become less stable. This can result in electrons relaxing to lower levels even if the incoming photons do

not exactly match the energy difference between the levels. As a result of this, the emitted photons may vary in energy and thus wavelength and causes the lasing bandwidth to be wider for high drive currents [10]. These variations in photon energy are often referred to as the stability of the laser.

The plasmatic effect refers to the changes in the refractive index of the material due to the changes in the current density. Increasing the current will result in an increase in the number of free electrons in the material. This increase in electron density increases the refractive index of the material which affects the lasing wavelength of the laser. At lower modulation frequencies the thermal effects tend to dominate the behavior of the laser diode [7] and because of this the plasma effect will be ignored during the foregoing of this project.

2.3 LiDAR link budget

LiDAR systems can be modelled as an optical link from the transmission from the laser to the receiver through free-space coupling and target reflection. The optical power that can be used in a LiDAR has constraints due to eye-safety considerations. This maximum power makes it possible to calculate the portion of light that is returned after hitting a target. The calculation is often referred to as link budget. Link budget takes into account the target reflection, coupling efficiencies, and beam divergence. It is also assumed that a certain number of photons are required in a given time to get a detectable signal [8, 9].

In this section the different components of the link budget will be estimated. The maximum output will be approximated according to eye-safety standards, the coupling efficiency will be approximated, lens characteristics and beam divergence will be modelled according to the "LiDAR range equation" [9] for use at optical wavelengths. Furthermore, FMCW LiDAR SNR and reflection loss due to Lambertian reflection will be considered.

2.3.1 Eye-safety standards

As mentioned in section 2.2.1, light sources of a wavelength of 1550 nm have become more commonly used in FMCW LiDAR applications. The wavelength of 1550 nm allows the use of an optical power several magnitudes higher than 905 nm. The increase in optical power is due to eye-safety considerations, which take into account retinal damage and corneal damage. As 1550 nm is not focused on the retina of the human eye, compared to 905 nm, the main issue is the damage of the cornea. This damage is due to absorbed light in the cornea and limits the amount of optical power that can be used in the proximity of humans without safety-wear [15].

The defined limits for safe use of lasers are dependent on the wavelength and are specified as "maximum permissible exposure" (MPE). MPE is measured in units of power or energy density of the light source and also differs depending on how it is operated (pulsed/CW). As the main focus in this project is based on FMCW, the effects of pulsed lasers will be ignored. For a 3.6 mm diameter aperture and an exposure time of 100 s, the maximum output power can be calculated according to equation 13 for a wavelength of 905 nm and equation 14 for a wavelength of 1550 nm [15]. The aperture size is chosen according to the dimensions of the collimators used in this project.

$$P_{max}(905\,\text{nm}) = MPE(905\,\text{nm}, 100\,\text{s}) \cdot \pi \left(\frac{3.6\,\text{mm}}{2}\right)^2 = 0.26\,\text{mW} \qquad (13)$$

$$P_{max}(1550\,\text{nm}) = MPE(1550\,\text{nm}, 100\,\text{s}) \cdot \pi \left(\frac{3.6\,\text{mm}}{2}\right)^2 = 10.19\,\text{mW} \qquad (14)$$

The MPE-values used in equations 13 and 14 are taken from *SVENSK STANDARD SS-EN 60825-1* [15]. These calculations support that lasers of wavelength 1550 nm allow a significantly higher optical power output compared to 905 nm and thus make 1550 nm a more favorable operating wavelength.

2.3.2 LiDAR range equation

To approximate the minimal optical power needed for detection at certain distances, LiDAR range equations are often used. The range equations have drastic variations depending on the type of LiDAR and the expected use. For this project the LiDAR range equation, equation 15, from *LiDAR Technologies and Systems* [9] will be used. The equation takes into account the divergence, surface reflectance, transmission medium, and the features of the system [9]:

$$P_S = P_T \frac{\sigma}{A_{illum}} \frac{A_{rec}}{A_{ref}} \eta_{atm}^2 \eta_{sys}, \qquad (15)$$

where P_S is the recieved signal, P_T is the transmitted power, σ is the cross-section in square meters, A_{illum} is the illuminated area, A_{rec} the receiver area, A_{ref} the effective average area illuminated by the reflection from the target, η_{atm} the atmospheric attenuation and η_{sys} the optical efficiency of the receiver system.

As can be seen, the LiDAR range equation consists of two ratios of areas. The first ratio is the cross-section divided by illuminated area, which in practice is $(1-\theta)\gamma$, where θ is the beam divergence in mrad and γ the reflectivity of the surface [10]. The second ratio is the area of the receiver divided by the effective illuminated area by the reflection from the target. For a circular receiver with an aperture diameter of D_{rec}, the receiver area can be written $A_{rec} = \pi(D_{rec}/2)^2$ and assuming that the target has a Lambertian surface, A_{ref} can be written as the surface area of a hemisphere with a radius equal to the distance to the target, R. Since a Lambertian surface reflects light with a cosine distribution, a cosine term needs to be added [9]. The atmospheric attenuation follows Beer–Lambert law and has an exponential decay following $\eta_{atm} = e^{-R\alpha}$, where R is the distance, α is the attenuation coefficient ($\alpha \approx 1$ for a wavelength of 1550 nm in Air at 20 °C) [10].

This allows equation 15 to be rewritten as equation 16:

$$P_S = P_T(1-\theta)\gamma \frac{\pi(D_{rec}/2)^2}{4\pi R^2/2} \cos(\varphi) e^{-2R\alpha} \eta_{sys} = P_T(1-\theta)\gamma \frac{D_{rec}^2}{8R^2} \cos(\varphi) e^{-2R\alpha} \eta_{sys} \quad (16)$$

The factor that affects the optical power the most is the distance to the reflective surface. This inverse-square relation results in the optical power dropping rapidly and thus increase the importance of the detector chosen for the system.

2.3.3 Fiber loss

Another element that may affect the optical power is losses due to the optical fibers. The attenuation in optical fibers results in an exponentially decreasing rate and limits the optical power transmitted through it. The attenuation factor is defined according to equation 17 [10]:

$$\alpha = \frac{1}{L} 10 \log_{10} \frac{P(L)}{P(0)}, \tag{17}$$

where L is the fiber length, $P(0)$ incident power and $P(L)$ the power transmitted through the fiber.

α is usually defined in the unit of dB/km and highly dependent on wavelength. For fused silica the attenuation factor at 1550 nm is approximately 0.15 dB/km. Solving equation 17 for the power ratio and inserting the $\alpha = 0.15$ dB/km, gives the equation 18 [10].

$$P(L)/P(0) = 10^{-\alpha L/10} \approx e^{-0.23\alpha L} = e^{-0.345L} \tag{18}$$

Thus, it can be concluded that for short distances the power loss due to attenuation is small. For a fiber of length 100 m the resulting power-loss will be 3.4 %, while it is only 0.35 % for a 10 m fiber. Hence, for LiDAR applications this factor can be neglected.

There are also different types of fiber connectors. The ones used in this project are FC/APC, which is an abbreviation for "Fiber-connector/Angled physical contact". FC/APC connectors minimize back-reflection due to an 8° angle-polish applied to end surfaces. This angle results in the reflected light not staying in the fiber core but is instead reflected out into the cladding. The reason for avoiding back-reflection to the laser source is that it may affect the overall performance of it, by affecting the stability of the central wavelength. By using FC/APC connectors the back-reflection can be decreased by more than 60 dB. The insertion loss which occurs when mating FC/APC with FC/APC is in the order of $0 - 0.2$ dB. For the highest insertion loss this indicates that roughly 96 % of the light is transmitted through the connector. However, due to improved manufacturing processes and connector designs the insertion loss is often much lower.

2.3.4 Signal-To-Noise Ratio in FMCW LiDAR

Signal-to-Noise Ratio (SNR) is a measure of the signal compared to background noise and is defined as the ratio of signal power to the noise power. To further support the claim of FMCW LiDAR having an advantageous resolution to ToF LiDAR, stated in section 2.1.1, the detector-limited SNR can be compared.

The optical power of the signal for ToF and FMCW LiDAR can be written as equation 19 and 20, respectively [12, 16]:

$$S_{ToF}^2 = \rho^2 P_S^2 \tag{19}$$

$$S_{FMCW}^2 = \rho^2 P_S P_{LO} \tag{20}$$

Here ρ is the responsivity of the PDs in A/W, P_s is the optical power of the signal and P_{LO} is the optical power of the LO.

The primary two sources of noise in a detector are current shot noise and thermal noise. Current shot noise arises due to the discrete nature of electrons and occurs at low photon flux due to the random arrival times of individual photons. Thermal noise is generated by thermal disturbances of the charged carriers in the detector and is a random effect dependent on the material. These two effects give rise to noise spectral density which has the unit A^2/Hz and is described by equation 21 and 22, respectively [8]:

$$\sigma^2_{Shot} = 2q \left(\rho B P_{DC}\right), \tag{21}$$

$$\sigma^2_{Thermal} = \frac{4kTB}{R}, \tag{22}$$

where q is the electron charge, P_{DC} is the DC component of the incident signal, k is the Boltzmann constant, T is temperature, R is the effective resistance, and B is bandwidth of the detector, which is the frequency at which the response drops to 50% of its value at DC.

In FMCW LiDAR the DC optical power is usually dominated by the local oscillator component, which allows the approximation of $P_{DC} \approx P_{LO}$. This results in a SNR for ToF and FMCW LiDAR according to equations 23 and 24 [10]:

$$SNR_{ToF} = \frac{\sqrt{\rho^2 P_S^2}}{\sqrt{\frac{4kTB}{R} + 2q \left(\rho B P_{DC}\right)}} \tag{23}$$

$$SNR_{FMCW} = \frac{\sqrt{\rho^2 P_S P_{LO}}}{\sqrt{\frac{4kTB}{R} + 2q \left(\rho B P_{LO}\right)}} \tag{24}$$

From these equations it can be concluded that the SNR can be improved for FMCW LiDAR by increasing the optical signal power until the shot noise starts to dominate the thermal noise. Since $P_{LO} \gg P_S$, further increase will not affect the SNR significantly. Measurements with FMCW thus becomes advantageous over ToF, as they become fundamentally limited by shot noise instead of the thermal noise of the detector.

Another source of noise is background radiation. Background radiation is fundamentally the same as undesired signals from sources other than the system and due to this it will be amplified along with the signal when detected. The most common source of background noise is solar radiation. The sun is a black body and the solar radiation spectrum thereby follow a typical black body radiation curve [9], shown in figure 7.

Solar background radiation can be considered a uniform radiation incident on the receiver. Thus, by applying balanced photodetection, section 2.2.2, this radiation will be split up into two correlated noise sources before incident on the detectors. Perfectly correlated noise sources will then cancel out when processed by the detectors, while partially correlated noise sources will be suppressed [17]. As can be seen in figure 7, the solar spectral irradiance (SSI) at sea level at 1550 nm is about $0.2 \, W/m^2/nm$ compared to $0.6 \, W/m^2/nm$ at 905 nm. This SSI may cause new sources of noise in a coherent detector. One is the increased shot-noise that may occur as the solar radiation increase P_{DC}. However, certain detection methods will eliminate or heavily suppress these sources.
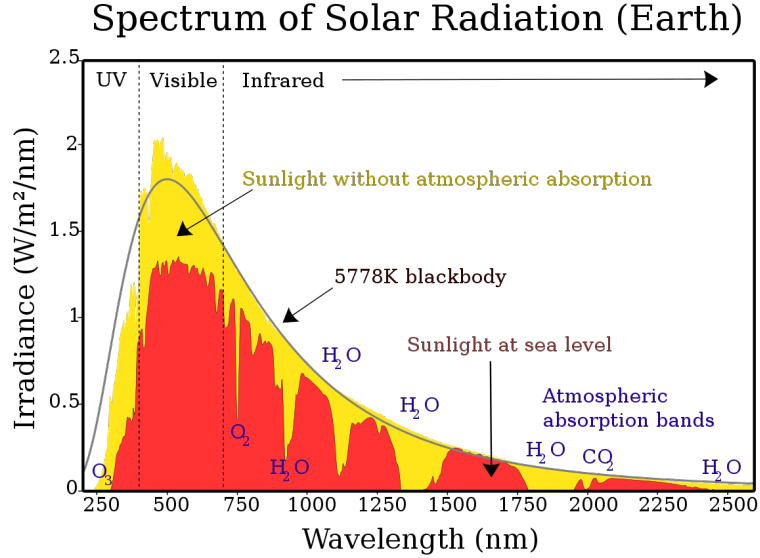
Figure 7: The figure shows the spectrum of solar radiation. The red is the radiation at sea level and the yellow is out of the atmosphere. As be seen, that the atmospheric absorption is very low at 1550 nm, compared to 905 nm, which causes a larger portion of solar radiation to reach sea level. The total SSI is, however, lower at 1550 nm than 905 nm, which leads to a less radiation at sea level at 1550 nm [18]

2.4 Coherence

Coherence is a characteristic that describes the properties of the correlation between physical quantities of waves. It is based on the statistical similarity of a field at two points in time (temporal coherence) and/or space (spatial coherence). FMCW (coherent) LiDAR utilizes the temporal coherence [9].

Temporal coherence represents how monochromatic a light source is. It characterizes how well a wave can interfere with itself at a delay and thus how the phase or amplitude shifts as the light propagates. The time it takes for this shift to cause the magnitude of the coherence function to drop to $1/e$ is called coherence time, T_{coh} [9]. It is however more common to talk about the coherence length, L_{coh}, which is the distance the wave travels in time T_{coh}. This is due to that T_{coh} often is determined by optical path length [10, 19].

The coherence length of perfectly monochromatic light is infinite everywhere. However, the perfect conditions for monochromatic light are not possible to achieve in practice. Instead the spectrum of light emitted from a source is confined to a narrow band around a center frequency. The width of this narrow band is called the linewidth, $\Delta\nu$, and is most commonly measured at full-width half-maximum (FWHM) of the spectral peak and has a relation to the coherence length which is dependent on the spectral profile. To show this dependence we can look at two common spectral shapes: Gaussian and Lorentzian. For a Gaussian line shape the coherence length can be estimated according to equation

25 and for a Lorentzian line shape it can be estimated according to equation 26 [10].

$$L_{coh} = \frac{c\sqrt{2\ln 2/\pi}}{\Delta v} \tag{25}$$

$$L_{coh} = \frac{c}{\pi\Delta v}, \tag{26}$$

where Δv is the linewidth at FWHM and c the speed of light. These estimates do not include the refractive index of the propagation medium. The refractive index may affect the coherence length heavily and should be considered when applied in practice.

3 Experimental setup and procedure

The process of designing a setup was one of the main parts of the project. The LiDAR was expected to measure the distance to a target placed up to 8-10 m away from the setup and be cost-efficient. Cost-efficient is a vague term that in practice states that the system should be to as low cost as possible, while fulfilling the performance requirement. The available budget was restrained to 50 000 SEK.
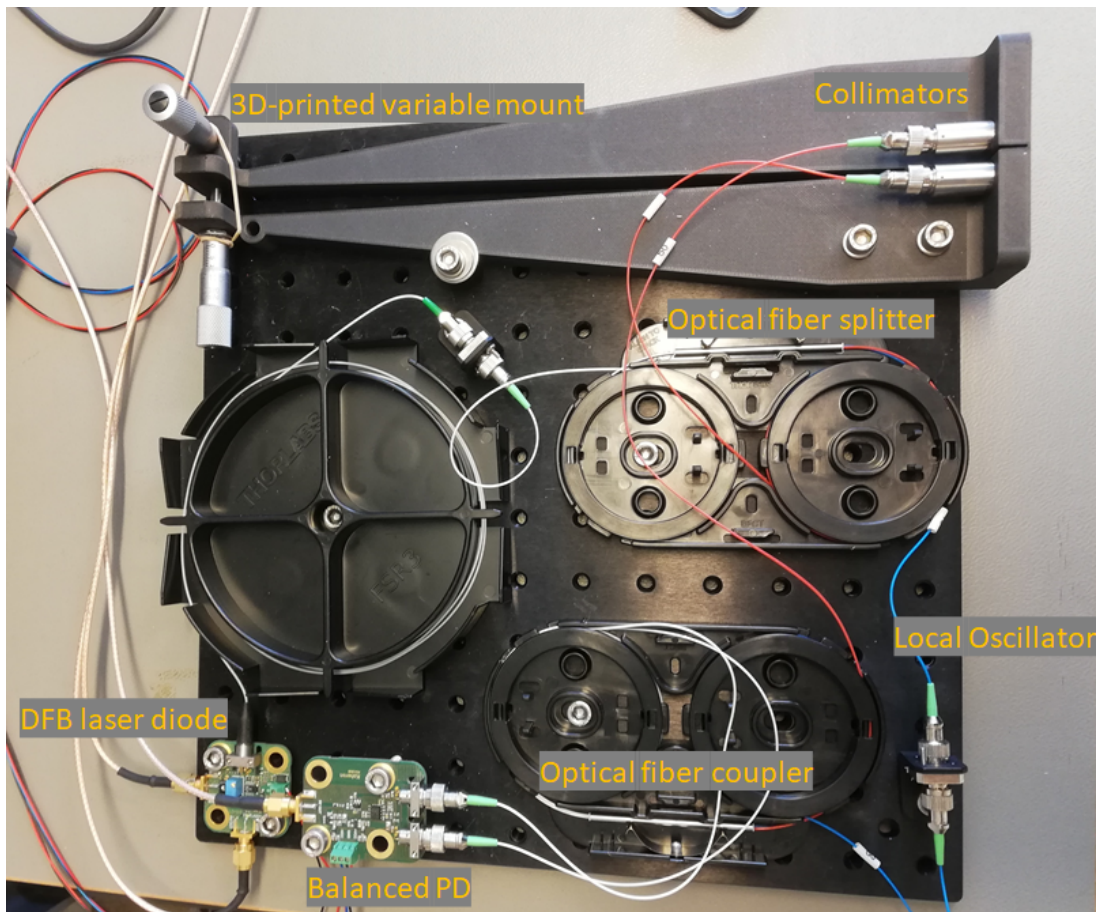
Figure 8: The figure shows the final setup used in the project. The setup consists of a DFB laser diode, two optical fiber couplers/splitters, two collimators, a balanced photodiode, a 3D-printed collimator mount and optical single mode fibers to connect all the components. The output from the photodiode was then observed on an oscilloscope.

The final setup used for this project is shown in figure 8, with a schematic of it shown in figure 9. The setup consisted of a waveform generator, a DC power supply, a light source in the form of a DFB laser diode, two optical fiber couplers/splitters, two collimators, a balanced photodiode, a collimator mount, an oscilloscope and optical single-mode fibers to connect all the components. The setup was designed as bi-static, meaning with two separate collimators, one for receiving and one for transmitting optical signal. The mount was designed and 3D-printed to facilitate the alignment of the collimators. The mount allowed for small adjustments both vertically and horizontally using two micrometer-screws built into the mount. The adjustment of the collimators was necessary as the angle between them affected the amount of optical signal that was captured by the system.

The DFB laser was directly fiber-coupled by the manufacturer and thus optimized to get the maximum amount of light into the fiber. As can be seen in figure 9, the light was then split into two different paths in a similar way as described in section 2.1.1. The length of the LO was 3.49 m while the length of the fiber along the signal arm was 3.54 m, including the length of the collimators. The light was then coupled to get interference between the signal and LO and finally separated into two fibers that directed the light onto the balanced photodetector. The output from the balanced photodetector was then observed on an oscilloscope which could perform a FFT directly on the signal.
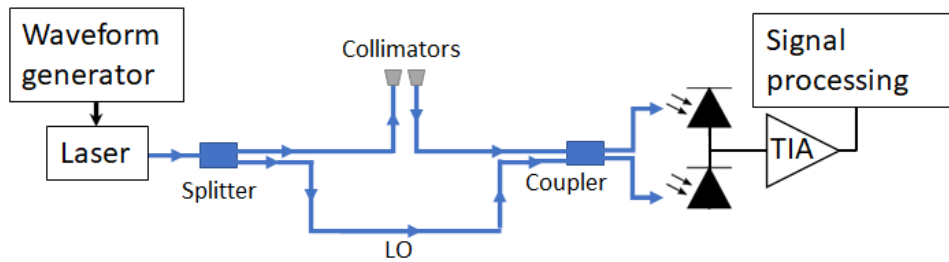

Figure 9: A schematic of the final setup used in the project (figure 8).

3.1 Components

The optical components used in the project are presented in table 1. As can be seen, the total cost for the optical components used was 10 297 SEK, which is within the budget. This is in the same price range as comparable industrial LiDARs with similar detection range. These industrial LiDAR do, however, contain signal processing and visual presentations that are not included in the cost of the optical components. When comparing to ToF LiDAR, the prices have larger variations. In general, the price of a ToF LiDAR is lower, mainly due to the use of simpler detectors as ToF LiDAR most commonly uses a PIN PD. The choice of laser wavelength does also affect the price with components for 1550 nm, such as laser diode, optical fibers, and detectors, having around 10-20% higher price.

Table 1: The optical components used in the setup with price, and Article name. The total price of the components is presented in the last row.

Component	Cost	Manufacturer	Article
Laser diode	3742 SEK	Koheron	LD101
Collimators (2 pieces)	3876 SEK	Thorlabs	F280APC-1550
Balanced Photodetector	2115 SEK	Koheron	PD100B
1x2 fiber coupler 90/10	163 SEK	Koheron	FOSPL12-9010
2x2 fiber coupler 50/50	130 SEK	Koheron	FOSPL22-5050
FC/APC connectors (10 pack)	271 SEK	Koheron	FOADA-A-A
Total	**10 297 SEK**		

3.1.1   Laser

The laser used in the project was a DFB laser diode with a central output wavelength of 1550 nm. The laser diode was mounted on a circuit with an integrated current driver and an internal photodetector, the schematic is shown in figure 10. The current driver was controlled by an AC-coupled modulation input and had a recommended operational supply power of 3.3 V, which was used during the project. The integrated photodetector had a built-in transimpedance amplifier with a gain of 2 V/mA and a bandwidth of 40 MHz.

The specification for the laser diode stated that it had a Lorentzian wave-profile width a linewidth of 5 MHz. Applying equation 26 gave a coherence length of 19.09 m. The optical path length for the fiber in the signal arm was $1.49 \cdot 3.49$ m $= 5.20$ m, where the 1.49 is the refractive index of fused silica. This indicates that the theoretically longest distance that could be measured with the setup was $(19.09$ m-5.20 m$)/2 = 6.95$ m, measured from the collimators taking into account that the light had to travel back and forth from the target. The laser was therefore assumed to have a coherence length enough for accurate measurements up to 7 m. This also indicates that the precision should decrease after 7 m. However, as mentioned in section 2.4, this is an estimation of the coherence length and therefore may vary.
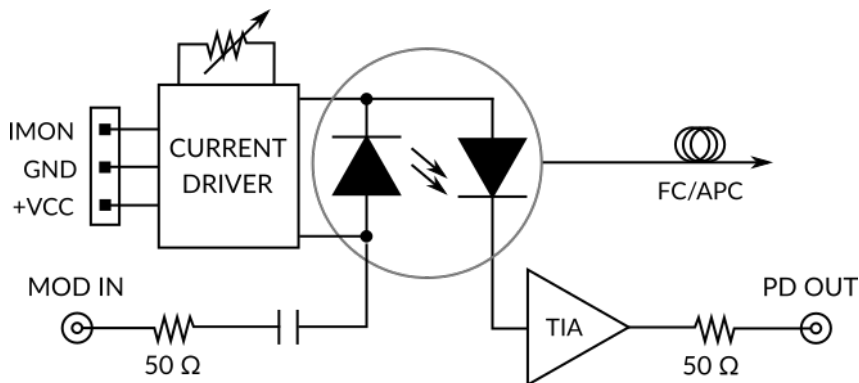

Figure 10: Schematic of the laser circuit used in the project [20].

3.1.2 Detector

As mentioned in section 2.2.2, the detector used for this project was a balanced photodetector. The detector was mounted on a circuit and consisted of two InGaAs photodetectors and a TIA, the schematic is presented in figure 11. The small-signal bandwidth of the detector was stated as 100 MHz, the transimpedance gain as 39 kV/A, and the CMRR as 35 dB. During the project a power supply of 6 V was applied to the +VCC pin and −6 V to the -VCC pin.
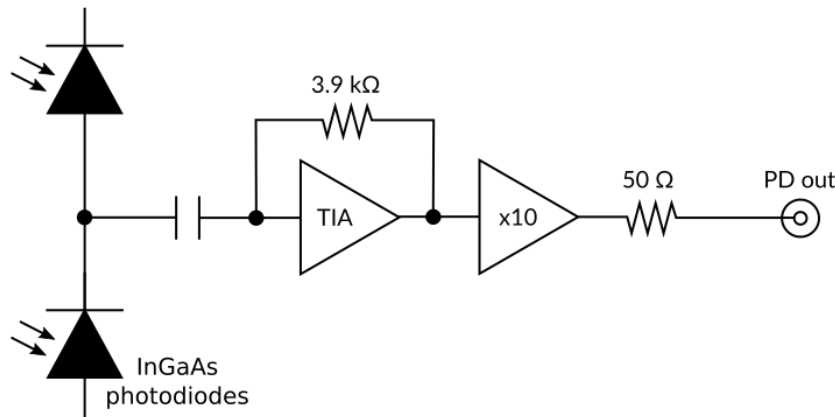

Figure 11: Schematic of the balanced photodetector used in the project [21]

3.1.3 Collimators

The collimators used in the project were fixed focus collimators with FC/APC connectors and constructed of an aspheric lens with a focal length of 18.75 mm and a numerical aperture of 0.15. The wavelength used for alignment was 1550 nm. The specification stated that the beam diameter at 1 focal length distance was 3.6 mm with a beam divergence of 0.559 mrad.

The collimators were suitable for both transmitting and receiving light. However, the setup could possibly have been improved by the use of a larger aperture for the receiver. This would have allowed a larger amount of the reflected signal to be collected but also increased the incident light from surrounding sources. The effects of using a collimator with a wider aperture as a receiver could be an interesting feature to investigate further.

3.2 Link budget

When calculating the link budget for the LiDAR system, consideration was taken to all the components as well as their effects according to section 2.3. The output power from the DFB laser diode was 4.1 mW. This was then divided up such that 3.7 mW (90 %) was used as the signal and 0.3 mW (10 %) as the LO.

Calculating with maximal possible losses, an insertion loss of 0.2 dB for each FC/APC connector was assumed. Thus, the optical power transmitted from the collimator was approximately 3.37 mW as it was transmitted through two FC/APC connectors. Inserting

this into the LiDAR range equation, equation 16, gave:

$$P_T = 3.37\,\text{mW} \cdot (1 - 0.558) \cdot 0.75 \frac{3.6\,\text{mm}^2}{8 \cdot 10^2} \cdot 0.90 = 1.63 \cdot 10^{-11}\text{W} = 16.3\,\text{pW} \qquad (27)$$

In this calculation it was assumed that the target had a reflectance of 75 % and was placed 10 m from the collimators. As the cosine term varies between 0 and 1, it was assumed to be 1 for convenience and the atmospheric attenuation was neglected. Furthermore, the optical efficiency of the receiver system is hard to approximate. For this project the peak responsivity stated by the manufacturer, $\eta_{sys} = 0.90$, was used as the optical efficiency.

The optical power received by the collimator was then transmitted through two FC/APC connectors. This results in optical power of 16.3 pW transmitted through the signal-arm of the LiDAR. The optical power through the LO was transmitted through three FC/APC connectors, which results in a remaining optical output of 0.26 mW.

As the optical power from the two arms was mixed and allowed to interfere, the total light incident in the PDs could be approximated according to equation 8 and resulted in:

$$P_{max} = \left(16.3\,\text{pW} + 0.26\,\text{mW} + 2\sqrt{16.3\,\text{pW} \cdot 0.26\,\text{mW}}\right) = 261.5\,\text{μW}$$
$$P_{min} = \left(16.3\,\text{pW} + 0.26\,\text{mW}\right) = 261.3\,\text{μW}$$

$$(28)$$

P_{min} was calculated for a cosine term equal to 0 and P_{max} for a cosine term equal to 1. The incident optical power of 261.3 μW is split onto two PDs and the photocurrent from the PDs becomes 117.6 μA, using the previously stated responsivity for the detector. This photocurrent was then converted to a voltage by the TIA with a gain of 39 kV/A. This conversion results in an output voltage of 4.59 V. Observed voltage on the oscilloscope was between 3-5 V implicating that the estimation is reasonable.

The noise that arise from the detector can be calculated according to equations 21 and 22 and gives:

$$\sigma^2_{Shot} = 2 \cdot (1.60 \cdot 10^{-19}\text{C}) \cdot 100\,\text{MHz} \cdot 0.26\,\text{mW} = 8.33 \cdot 10^{-15}\text{A}^2, \qquad (29)$$

$$\sigma^2_{Thermal} = \frac{4 \cdot (1.38 \cdot 10^{-23}\text{m}^2\text{kgs}^{-2}\text{K}^{-1}) \cdot 100\,\text{MHz}}{10\,\text{MΩ}} = 5.52 \cdot 10^{-22}\text{A}^2, \qquad (30)$$

where the resistance of the detector is approximated by a shunt resistance of 10 MΩ. The integrated TIA also contributes to noise that should be included. The TIA noise consists of thermal noise and can thus be calculated according to equation 22 and gives:

$$\sigma^2_{Thermal-TIA} = \frac{4 \cdot (1.38 \cdot 10^{-23}\text{m}^2\text{kgs}^{-2}\text{K}^{-1}) \cdot 100\,\text{MHz}}{3.9\,\text{kΩ}} = 1.41 \cdot 10^{-18}\text{A}^2. \qquad (31)$$

The SNR is then calculated according to equation 24 and becomes:

$$SNR = \frac{\sqrt{(0.9\,\text{A/W})^2 \cdot 16.3\,\text{pW} \cdot 0.26\,\text{mW}}}{\sqrt{8.33 \cdot 10^{-15}\text{A}^2 + 5.52 \cdot 10^{-22}\text{A}^2 + 1.41 \cdot 10^{-18}\text{A}^2}} = \frac{5.86 \cdot 10^{-8}\text{A}}{9.13 \cdot 10^{-8}\text{A}} = 0.64 \quad (32)$$

This indicates that the acquired signal from a target with 75% reflectance at a distance of 10 m will be smaller than the noise in the system. This is consistent with the theory,

which implicates that the maximum distance that could be measure is $7\,\mathrm{m}$. The low SNR results in the interference fringes, or beat frequency, disappearing into the noise. For better SNR, the beat frequency will arise as oscillations on the LO. These oscillations are shown in figure 12, where there is an overall triangular wave arising due to the frequency modulation of the LO and oscillations occurring due to interference with the signal.

In this case, the calculations are, however, done with maximum possible loss in the system. This is most probably not the case in practice and therefore it may be possible to get a higher optical power of the signal and thus improve the signal to noise ratio. It can also be seen that the shot noise is the dominating noise and thus, increasing the optical power of the LO will not improve the SNR significantly, as discussed previously (see Eq. 24).

3.3 Frequency modulation

When the components in the LiDAR system was in place, the modulation had to be configured. The original modulation was a triangular wave modulation, according to the theory described in section 2.1.1. However, when applying such modulation to the laser diode, the observed beat frequency on a static target was not constant. This non-constant result can be seen in figure 12, the distance between the interference fringes should show an equidistant behavior which indicates the beat frequency between the signal and the LO. However, the distance between the fringes differed, with wider apart just after the modulation shifts from down-chirp to up-chirp and then smaller distances until it shifts from up-chirp to down-chirp. Hence, the linear current modulation gave a non-linear frequency modulation resulting in an increase in the beat frequency during the chirp.
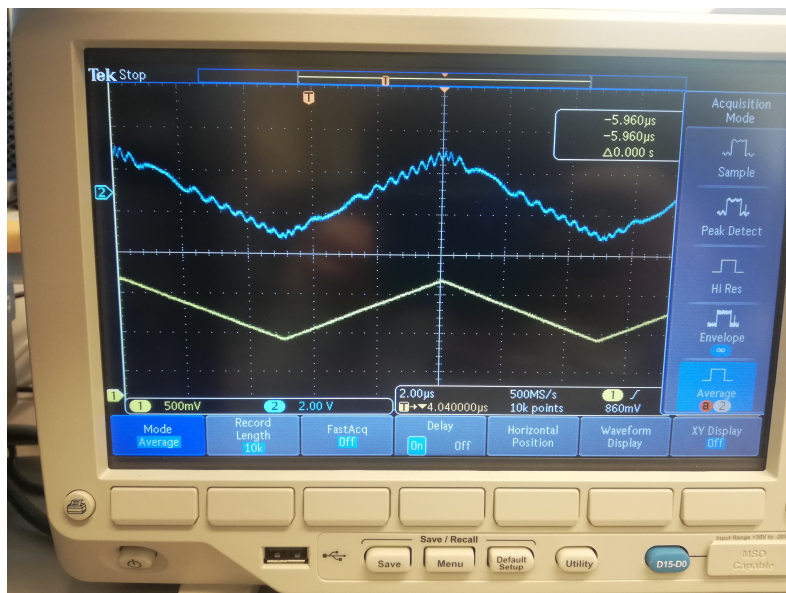

Figure 12: The figure shows the oscilloscope output for the triangle frequency modulation. The interference fringes occur with a non-constant distance between each other, which indicates a non-linear frequency modulation. The amplitude of the interference fringes, is dependent on the strength of the signal in relation to the LO. For this figure, the target was placed at $2\,\mathrm{m}$. This results in a optical power of $0.41\,\mathrm{nW}$ for the signal vs. $0.26\,\mathrm{mW}$.

This phenomenon most probably arose due to a delay in the response of the laser diode. This delay made the laser diode have an exponential behavior when shifting chirp, similar to the one illustrated in figure 6. To compensate for this behavior the modulation function was modified. The most optimal way to compensate would be to model the thermal behavior of the laser diode. The specifications provided by the manufacturer were limited and such a model could not be performed due to the time limitation of the project. Instead a compensation function was created. This was done by creating an arbitrary waveform for the frequency modulation.
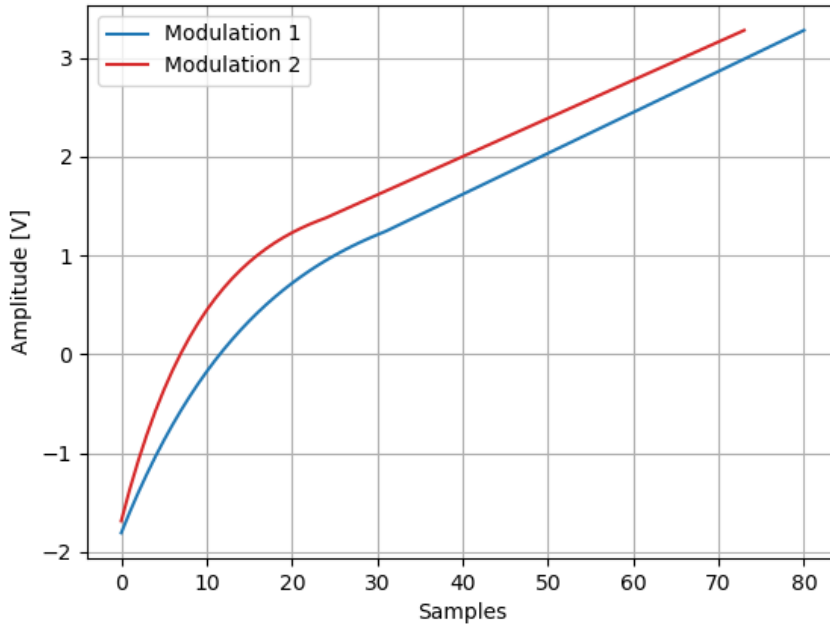
Figure 13: The figure shows two of the functions tested as compensation functions for the frequency modulation. *Modulation 2* (red) was function with most consistent distance between the interference fringes and thus chosen as compensation function.

Multiple different arbitrary waveforms were tested as compensation functions, figure 13 shows two of them. The generation of these functions was an iterative process of trial and error. The functions started with a rapid increase in an attempt to make the diode reach the stable state sooner. The compensation function that resulted in the most consistent distance between the interference fringes was *Modulation 2*, presented in figure 13. To further investigate the performance of the arbitrary functions as compensation functions, distance measurements were made on a target with an $80\,\%$ reflectance between 1-7.5 m. This was done to see how the precision varied with distance and thus determine which modulation was most reliable. The result for the two functions in figure 13 is shown in figure 14.

Figure 14 shows fitted linear functions to the data points of the measured distance vs the actual distance for functions *Modulation 1* and *Modulation 2* presented in figure 13. The fitted function for *Modulation 1* is $y = 1.200x - 0.0009$ while the fitted function for *Modulation 2* is $y = 1.005x + 0.0064$. This indicates that the measurement error of

Modulation 1 will increases with 20 cm for every 1 m increase in distance, while the measurement error of *Modulation 2* increases with 0.5 cm. The result further supports the use of *Modulation 2* as compensation function and *Modulation 2* was therefore selected as the compensation function. The chirp-rate of this function was 124.37 THz/s.
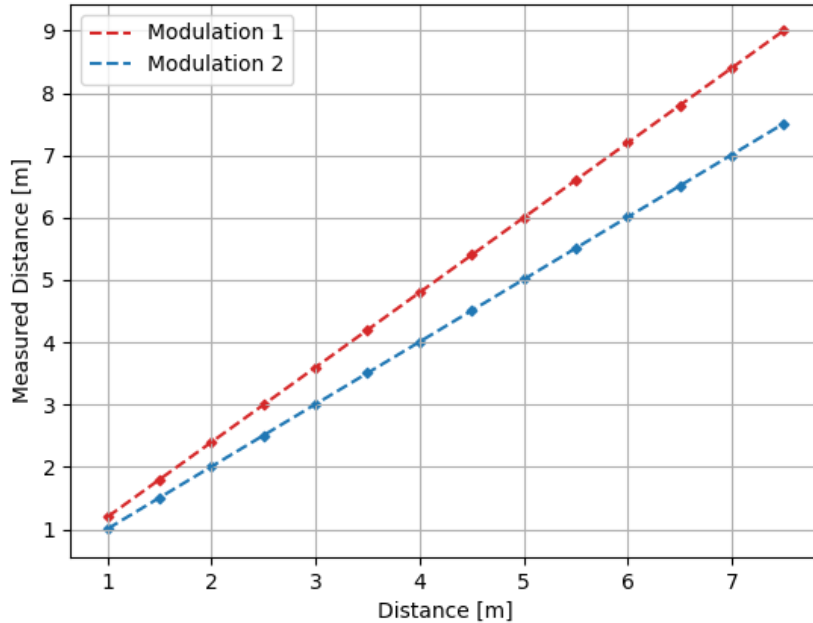

Figure 14: The figure shows the fitted linear functions to the data points of the measure distance vs the actual distance for functions *Modulation 1* and *Modulation 2* presented in figure 13.

3.4 Measuring construct and procedure

The targets were placed in a holder that was designed such that it could slide along a rail placed on the floor, see figure 15. The rail was placed such that distances between 2.5 m to 10 m could be measured. The rail allowed for the targets to be at the same distance, height, and angle when moved along the line of sight of the LiDAR.

Two different measurement series where taken. The first consisted of measurements on five plates with reflectances of 75%, 50%, 30%, 10%, and 5% respectively, figure 16. The first distance that were measured where 2.5 m. One measurement was taken for every plate and then the holder was moved 0.5 m further away from the LiDAR and new measurements were taken. This procedure was done up to a distance of 10 m and repeated five times. The second measurement series were taken on six different materials: wood, bubble wrap, cotton, Masonite, dark fabric, and ice. The measurements where all taken at a distance of 2.5 m and repeated 5 times.

The measurement-data consisted of data from the FFT spectra for each of the taken measurement. The data was then analyzed by identifying the frequency peak corresponding to the beat frequency that occurred due to the reflection of the targets.

Figure 15: The figure shows the rail with holder for the targets. The rail was placed such that distances between 2.5-10 m could be measured. The first distance that where measured where 2.5 m. One measurement where taken for every plate and then the holder was moved 0.5 m further away from the LiDAR and new measurements where taken.
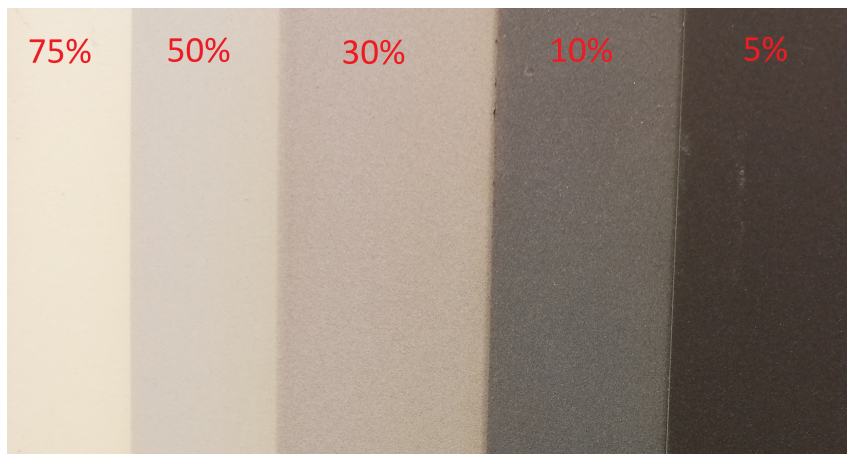
Figure 16: The figure shows the reflectance plates that was used as targets when measuring. All plates where made of the same material with different colors/coatings, which resulted in different reflectance.

4 Result and Discussion

To determine the precision of the LiDAR when measuring distance, the difference from the actual distance was analyzed, in this report this is referred to as *deviance*. This was done for distances between 2.5-10 m for five plates with different reflectance: 5%, 10%, 30%, 50%, and 75%. The measurements where taken for every 0.5 m for each of the plates and the mean, median, and standard deviation was calculated. The results for the mean deviance for all of the plates can be seen in figure 17. The increased deviation that occurs due to the compensation function is accounted for by subtraction and a positive deviance corresponds to the LiDAR showing a longer distance than the measured distance.

The measurements for the reflectance plate with 5% reflectance consists of fewer data point. This comes from that peaks at distances above 7 m was not possible to identify. As declared in section 3.1.1, 7 m was the distance where the precision was expected to decrease due to the coherence of the light. As a result in the light becoming less coherent the frequencies contained in the light will be spread over a larger interval causing the spectral linewidth of the laser to be broadened. This causes the central peak to have a much lower amplitude. In the case of a target with a 5% reflectance the amplitude is so low that it could not be separated from the noise. Thus, it can be concluded that the laser linewidth, the coherence, or optical power must be improved to be able to take these measurements. This decrease in precision can also be seen for the other plates were the deviance increase slightly faster after 7 m than before. The 30% and 50% reflectance plates follow the same pattern. This is an interesting behavior that indicates that these reflectance levels do not affect the deviance significantly. However, as the measurements are only taken for distances up to 10 m, they may separate for longer distances. It is thus expected to the 30% plate to show a faster increase in deviation than the 50% plate if measured at longer distances.

The overall trend in figure 17 is increasing deviance as the distance increase. This is consistent for all the plates but more prominent for lower reflectance. The deviances for the plates have high fluctuations. These fluctuations arise due to numerous factors such as imperfections in the compensation function, variations in surrounding light sources, the temperature of the laser diode, etc. One of the most prominent factors might be the stability of the laser diode. As mentioned in section 2.2.3, the laser diode is highly reliant on the grating structure in the active layer. As the temperature changes with the applied voltage this may affect the central wavelength of the emitted light in a way that the compensation function does not include. For example, the DFB laser diode may mode-jump at certain drive currents. If the jump is small enough it would be hard to directly notice in the spectrum but may affect the result significantly. Mode-jumping is a commonly known feature in semiconductor lasers and may cause the wavelength to make discrete jumps at some temperatures. For this project, the variations in the drive current were however low and thus making mode-jumping unlikely.

Looking at the median deviance for individual plates the trend is further supported. As can be seen in figure 18, which shows the result for the individual plate with a reflectance of 30%, there are large variations in the deviance at the measured distances. The standard deviation is represented as the error-bars in figure 18 and are smaller for shorter distances than for large distances. This indicates a decreased precision for the
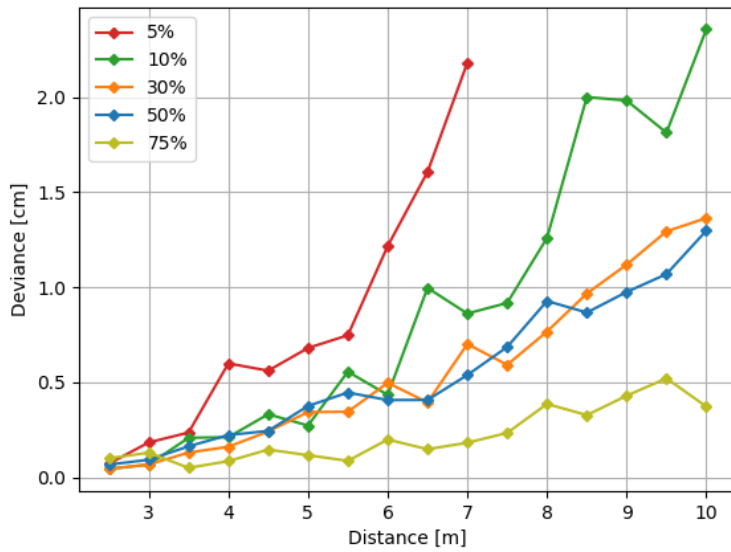
Figure 17: The figure shows the median deviance plotted against the measured distance for the five reflectance plates 5% (red), 10% (green), 30% (orange), 50% (blue), 75% (yellow). The deviance tends to increase as the measured distance increase. For the plates with lower reflectance the deviance increase faster.
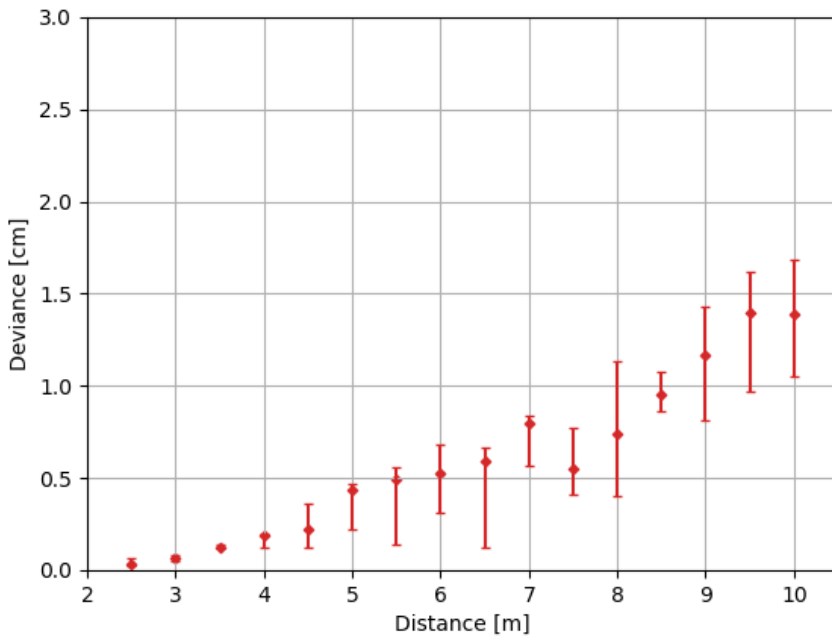

Figure 18: The figure shows the mean deviance plotted against the measured distance for the 30% reflectance plate. The error bars represent the standard deviation. There is a trend with higher deviance for longer distances.

LiDAR as the distance to the target increases, which is supported with similar behavior for all the reflectance plates (the individual results for the 5%, 10%, 50%, and 75% can be found in appendix A). The decreased precision is, as mentioned above, primarily an effect of the decreased coherence of the light.

The result presented in figure 17 implicates that the amount of light reflected from the target highly impacts the precision of the LiDAR. This implication arises as the deviance rises much faster for the plates with lower reflectance. To further support this implication, the amplitudes of the plates were plotted against the measured distance, figure 19. As can be seen in figure 19, the amplitude drops for all the plates as the distance becomes longer. This is expected as the beam diverges more the longer it travels. The beam divergence causes less light to be reflected into the collimator collecting the signal and thus the amplitude of the interference peaks to become lower.
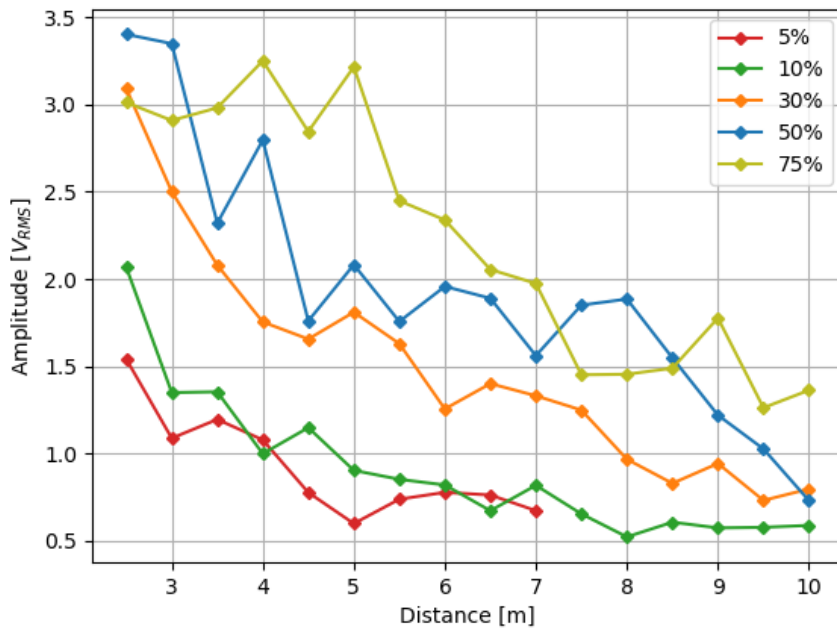

Figure 19: The figure shows the median amplitude plotted against the measured distance for the five reflectance plates 5% (red), 10% (green), 30% (orange), 50% (blue), 75% (yellow). The deviation tends to increase as the measured distance increase. The for plates with lower reflectance the deviation increase faster.

The over-all trend shows, as expected, that the plates with lower reflectance have a lower amplitude. Again, there are high fluctuations in the graphs which can be explained by numerous factors, most probably the alignment of the collimators. The reason for the alignment to be the most probable is that the collimators were manually aligned for each distance. This causes the amplitude to be highly dependent on the human factor. The alignment was done by moving the collimators vertically as well as horizontally with micrometer screws integrated to the mount. For each repetition of the measurement, this had to be done. As a result of this the collimators may not have been in an optimal position whenever the measurements were taken. As a result of this the amount of light

collected may have been heavily affected and thus the amplitude. Since, the measurements were repeated multiple times, this error should however have been compensated for. By comparing mean and median it can be seen that there is no distinct difference, which indicates that the data have a reasonable distribution.

The relationship between deviance and amplitude is shown in figure 20. As expected, the amplitude is higher for smaller deviance. The fitted line represents the function $y = 0.1306 + 0.5190/x^2$ and shows that there is an inverse-squared relation between the deviance and amplitude. The inverse-square law can be found in the LiDAR range equation, equation 16, and arise due to the point-source (collimator) radiating into a three-dimensional space. As the emitted light travels farther from the source, it spreads over an area that increases with the distance. The proportion of this increase is the square of the distance from the source and thus the intensity of radiation passing through any unit area is inversely proportional to the square of the distance from the point source. Investigating figure 17, this inverse-square relation can distinctly be seen for the plates with reflectance 5% and 10%, while it is not as clear for the other plates. If measurements had been taken at distances longer than 10 m it can be expected that the relation would have been seen more evidently for all the reflectance plates.
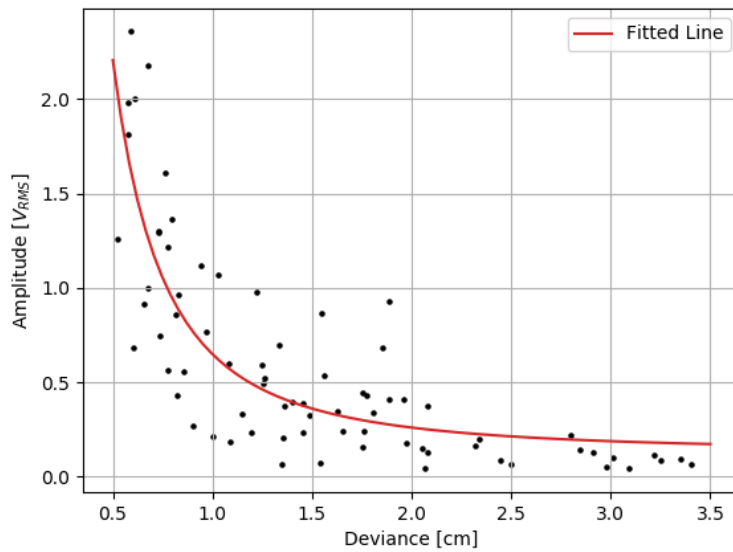

Figure 20: The figure shows the mean amplitude plotter against the mean deviation for all measurements with the five reflectance plates. The red line represents the fitted function $y = 0.1306 + 0.5190/x^2$. The fitted function indicates that there is an inverse-square law between the amplitude and the deviation from the measured distance.

The second measurement series was taken for different materials. The goal was to investigate if the material of the target affected the precision of the LiDAR system. The materials that were measured were: cotton, bubble wrap, dark fabric, Masonite, ice, and wood. The result can be seen in figures 21 and 22. All measurements were done at a distance of 2.5 m, as the result in the first measurement series showed that the precision was good at this distance. In figure 21 it can be seen that the mean deviances for the

materials are consistent between 0.4-0.5 cm for all materials except ice, which has a difference of 0.2 cm. The standard deviation, represented as error bars, is overlapping for all the materials, resulting in that no significance can be concluded. Therefore, it is implied that the LiDAR systems precision is not dependent on the type of material the target is composed of.
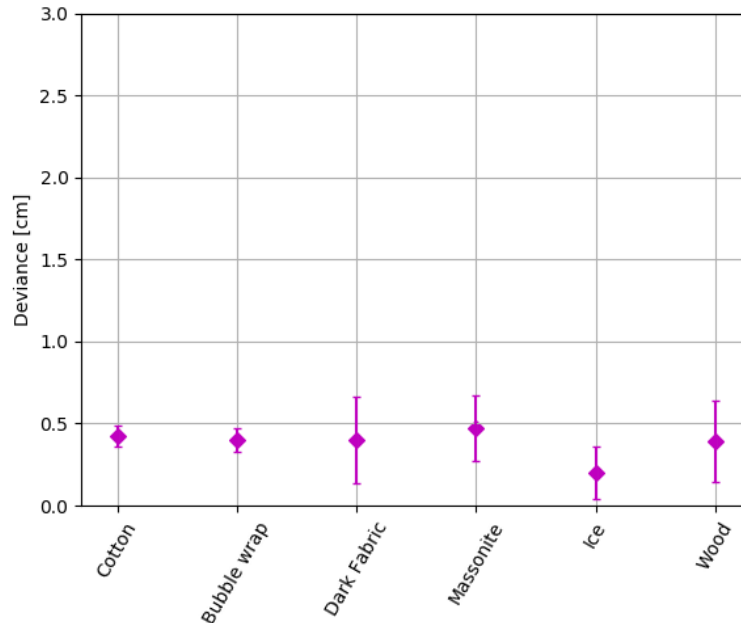

Figure 21: The figure shows the mean deviance for the materials: cotton, bubble wrap, dark fabric, Masonite, ice and wood. The measurements were taken at a distance of 2.5 m. The standard deviation for the measurements are presented as the errorbars.

To further support this, the amplitude for the materials was investigated, figure 22. As can be seen, the mean amplitudes have large variations depending on the materials, most probably due to different materials having different reflectance. Another factor that may affect the amplitude is polarization. The polarization has a large impact in the Fresnel equation, which describes the reflection and transmission of light in different mediums. To get a better understanding of the effects that polarization has, studies using different polarization-filters could be done.

The results in this section show that it was possible to design and setup a functioning LiDAR system. The cost and performance for such LiDAR might vary depending on the components used. For the specific design used in this project, the performance could have been improved further. Factors that should be further investigated to improve the LiDAR are the laser source and collimators.

As previously mentioned, the coherence length heavily affects the precision of the LiDAR. Thus, choosing a laser with longer coherence length is a simple way to improve the measurement precision. Furthermore, the materials used in the diode laser are not known for this project. This knowledge could help with modeling the thermal behavior

that occurs when varying the drive current. A thermal model would give a better way to compensate for the non-linear frequency modulation than the compensation function used during this project. The optical power of the laser is also a feature that may be increased. As shown in figure 20, the amplitude has an inverse-square relation with the deviance. Thus, by increasing the amplitude the precision might also be improved.

The dimensions of collimators that are used for transmitting and receiving the signal is another big factor to investigate further. This was briefly mentioned in section 3.1.3 as something to include in future projects. A larger receiver, for example, should give a larger amount of light collected. This, thereupon, lead to the signal more easily interfering with the LO and thus a larger amplitude for signals that may otherwise be to small to distinguish from the noise.
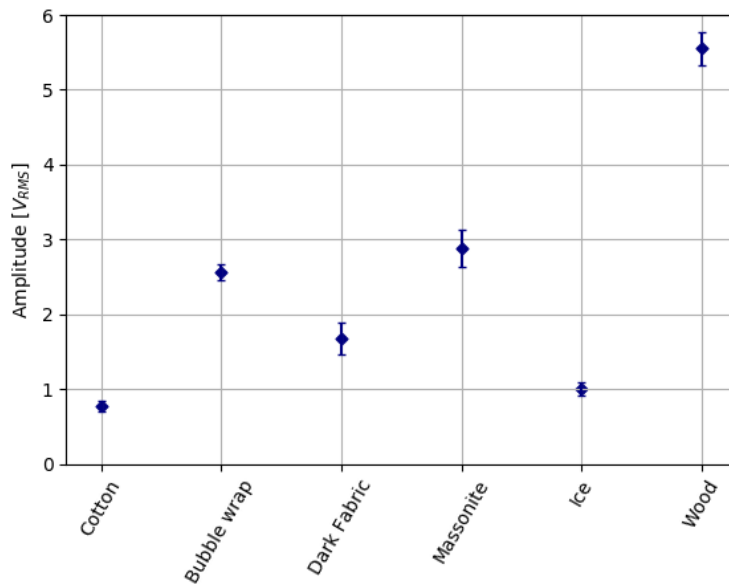

Figure 22: The figure shows the mean amplitude for the materials: cotton, bubble wrap, dark fabric, Masonite, ice and wood. The measurements were taken at a distance of 2.5 m. The standard deviation for the measurements are presented as the errorbars.

5 Conclusion

The results from this project shows that it is possible to design and construct a functioning FMCW LiDAR that can measure distances up to 10 m to a cost of around 10 000 SEK. This cost do not include power supply, signal analysis and visual presentation, which can have high costs. Furthermore, it can be concluded that the performance of such a Li-DAR system is highly dependent on the components used in the design. The light source, receiver system, and detector are three of the most important components for a system following the design used in this project.

For the light source, a laser diode emitting a wavelength of 1550 nm is the most convenient choice due to eye-safety considerations. The coherence length of the light source is another factor that is highly important and should be sufficiently long for the intended application. To increase the precision of the LiDAR a laser with smaller spectral linewidth could be used. The smaller linewidth increases the coherence length and thus allows for measuring longer distance with higher precision. It is also important to integrate a reliable method of frequency modulation. One possible way is through the drive current which affects the lasing wavelength of a laser diode.

The dimensions of both the collimator used for transmitting the signal and the component used as the receiver impact the optical power the system needs to function. The collimator will affect the divergence of the light and thus result in a lower or higher amount of light being reflected in the right direction. The dimensions of the receiver will in turn affect the amount of reflected light that is collected by the system. Using optics with shorter focal length is one approach that would allow the system to capture more radiation. Furthermore, other transmitting and receiving mechanisms may be more efficient and to investigate this part of the LiDAR can heavily improve the performance as well as lower the cost.

Using balanced photodetection the optical power needed for the signal can be decreased significantly. This allows for detection with precision much better than simple photodetection of targets with low reflectance as less reflected light is needed. Operating at low optical power levels is important when considering integration of photonics in electronics, since large amount of power in small chip is not desirable. Balanced photodetectors do, however, result in a higher cost.

The applications for FMCW LiDAR is highly flexible. One example is the autonomous vehicles industry that is currently investing millions of dollars in developing LiDAR technology. The LiDAR designed in this project is, however, far from the leading manufacturers' performance levels, but the goal of increasing the understanding of FMCW LiDAR systems has definitely been accomplished. The next step to increase the performance of FMCW LiDAR are investigations of the components mentioned above. Such investigation could result in FMCW LiDAR becoming the standard technique used for detection and ranging.

References

[1] J. Nunes-Pereira Eduardo et al. "The LiDAR hop-on-hop-off route: visiting the LiDARs past, present, and future landscapes". In: *Proc.SPIE*. Vol. 11207. DOI: 10.1117/12.2530904.

[2] V. Molebny et al. "Laser radar: historical prospective—from the East to the West". In: *Optical Engineering* 56.3 (2016), p. 031220. DOI: 10.1117/1.OE.56.3.031220.

[3] C Rablau. *Lidar: a new self-driving vehicle for introducing optics to broader engineering and non-engineering audiences*. Vol. 11143. Fifteenth Conference on Education and Training in Optics and Photonics: ETOP 2019. SPIE, 2019. DOI: 10.1117/12.2523863.

[4] B. Behroozpour et al. "Lidar System Architectures and Circuits". In: *IEEE Communications Magazine* 55 (2017), pp. 135–142. DOI: 10.1109/MCOM.2017.1700030.

[5] A. Elghandour and C. Ren. *Modeling and comparative study of various detection techniques for FMCW LIDAR using optisystem.* Vol. 8905. ISPDI 2013 - Fifth International Symposium on Photoelectronic Detection and Imaging. SPIE, 2013. DOI: 10.1117/12.2034878.

[6] J. Hecht. "FMCW lidar: An alternative for self-driving cars". In: *Laser Focus World* 55.5 (2019), pp. 22–25. ISSN: 10438092.

[7] D. Nordin. "Optical frequency modulated continuous wave (FMCW) range and velocity measurements". In: *Doctoral thesis* (2004). URL: http://urn.kb.se/resolve?urn=urn:nbn:se:ltu:diva-25907.

[8] P. Sandborn. "FMCW Lidar: Scaling to the Chip-Level and Improving Phase-Noise-Limited Performance". In: UCB/EECS-2019-148 (2019). URL: http://www2.eecs.berkeley.edu/Pubs/TechRpts/2019/EECS-2019-148.html.

[9] P. F. McManamon. *LiDAR Technologies and Systems.* SPIE / International Society for Optical Engineering, 2019. ISBN: 9781510625396. DOI: 10.1117/3.2518254.

[10] B. E. A. Saleh and M. C. Teich. *Fundamentals of photonics.* 2. ed. Wiley series in pure and applied optics. Wiley, 2007. ISBN: 9781299188952.

[11] T. Du Bosq and B. Preece. *Frequency modulated continuous wave lidar performance model for target detection.* Vol. 10178. SPIE Defense + Security. SPIE, 2017. DOI: 10.1117/12.2265712.

[12] X. Shi et al. "All-fiber coherent laser image Lidar based on phase correction". In: *Optics Express* 27.19 (2019), pp. 26432–26445. DOI: 10.1364/OE.27.026432.

[13] A. Beling and J. C. Campbell. "Chapter 3 - Advances in Photodetectors and Optical Receivers". In: *Optical Fiber Telecommunications (Sixth Edition).* Ed. by Ivan P. Kaminow, Tingye Li, and Alan E. Willner. Boston: Academic Press, 2013, pp. 99–154. ISBN: 15575837. DOI: 10.1016/B978-0-12-396958-3.00003-2.

[14] Newport Corporation. *Laser Diode Technology.* [Online; accessed April 27, 2020]. 2020. URL: https://www.newport.com/t/laser-diode-technology.

[15] Svensk Elstandard. "Laser - Säkerhet - Del 1: Klassificering av utrustning samt fordringar". In: *SVENSK STANDARD SS-EN 60825-1* (2014).

[16] Z. Xu et al. "FMCW Lidar Using Phase-Diversity Coherent Detection to Avoid Signal Aliasing". In: *IEEE Photonics Technology Letters* 31.22 (2019), pp. 1822–1825. DOI: 10.1109/LPT.2019.2948471.

[17] D. J. Lum, S. H. Knarr, and J. C. Howell. "Frequency-modulated continuous-wave LiDAR compressive depth-mapping". In: *Optics Express* 26.12 (2018), pp. 15420–15435. DOI: 10.1364/OE.26.015420.

[18] Wikimedia Creative Commons. *Solar spectrum.* [Online; accessed April 30, 2020]. 2019. URL: https://commons.wikimedia.org/wiki/File:Solar_spectrum_en.svg.

[19] P. A. M. Sandborn et al. "Dual-sideband linear FMCW lidar with homodyne detection for application in 3D imaging". In: *Conference on Lasers and Electro-Optics (CLEO).* 2016, pp. 1–2.

[20]   Koheron. *1550 nm low-noise DFB laser*. Datasheet LD101. [Online; accessed May 3, 2020]. URL: https://www.koheron.com/photonics/ld101-laser.

[21]   Koheron. *100 MHz balanced photodetector*. Datasheet PD100B. [Online; accessed May 3, 2020]. URL: https://www.koheron.com/photonics/pd100b-photodetection.

Appendix A: Deviance vs Distance
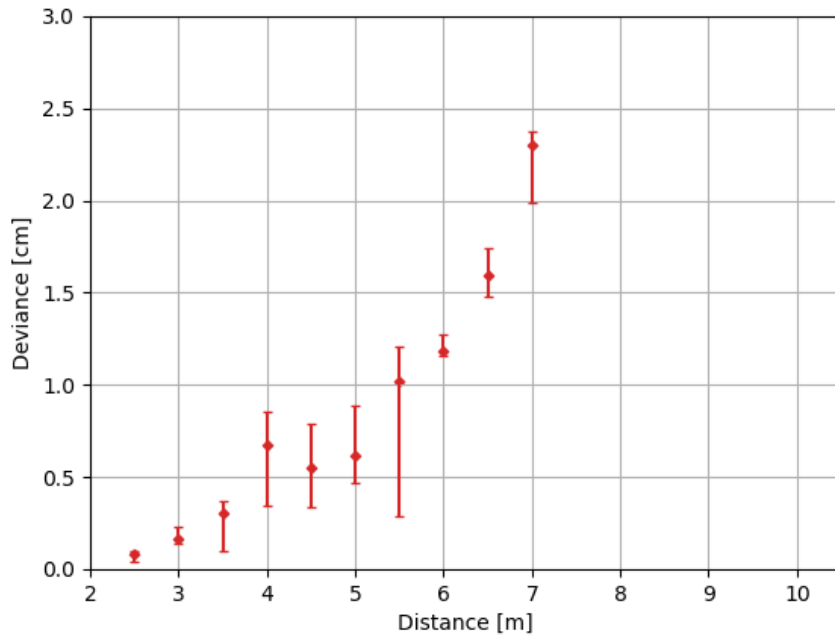
Figure 23: Individual result for the measurements with 5%-reflectance plate.
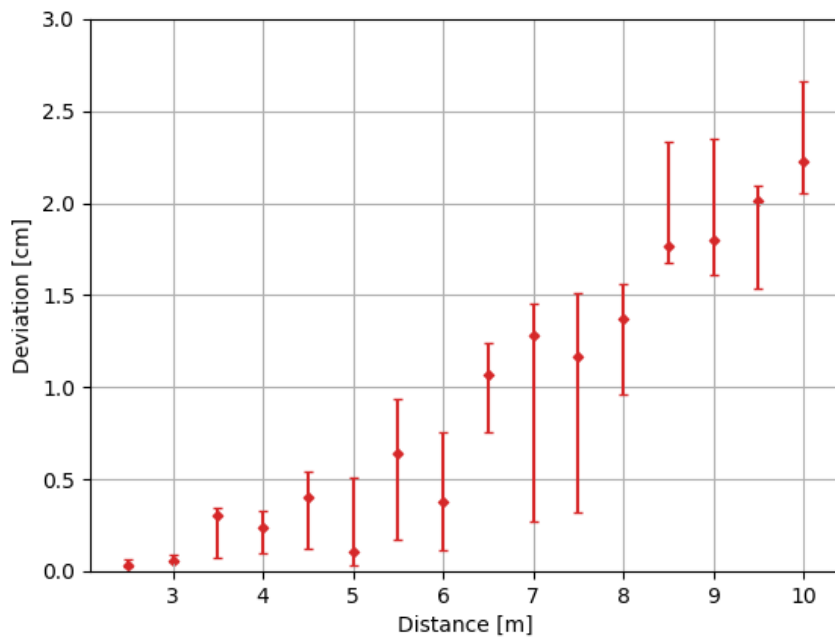
Figure 24: Individual result for the measurements with 10%-reflectance plate.

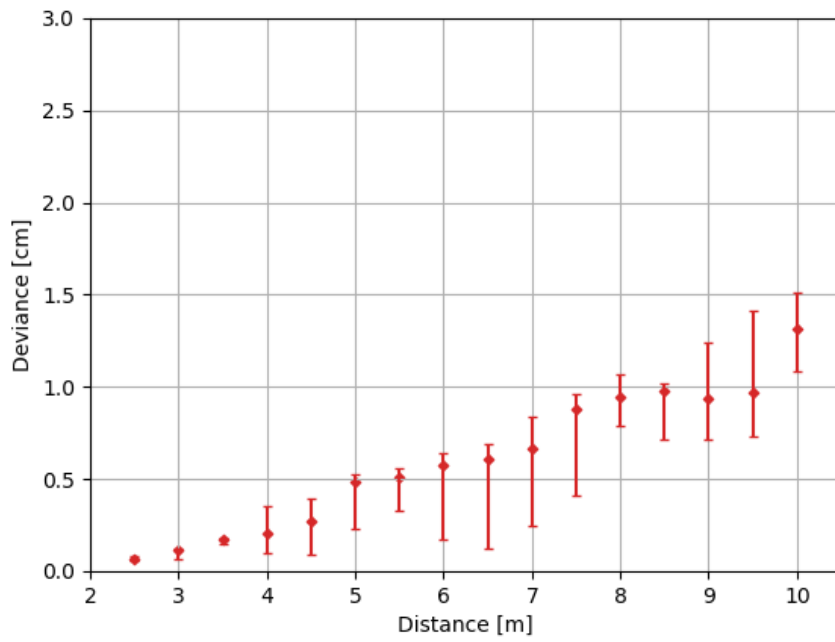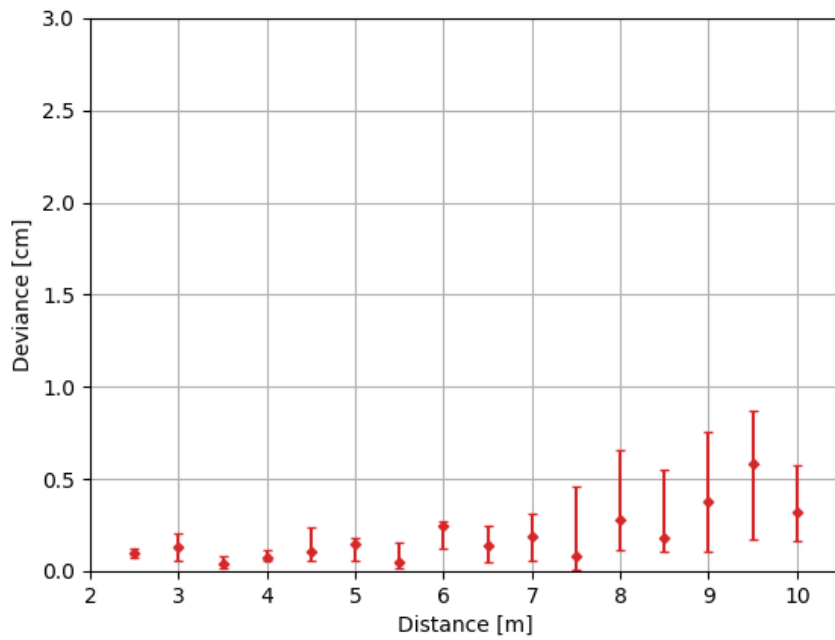**Figure 25:** Individual result for the measurements with 50%-reflectance plate.

Figure 26: Individual result for the measurements with 75%-reflectance plate.